Pedersen, R.B., Christie, D.M., and Miller, D.J. (Eds.)
Proceedings of the Ocean Drilling Program, Scientific Results Volume 187

2. Mineral Compositions of MORB from the Australian Antarctic Discordance (AAD): Implications for Mantle Source Characteristics[1]

Hiroshi Sato[2]

ABSTRACT

The chemical compositions of olivine, plagioclase, pyroxene, and spinel in lavas collected during Ocean Drilling Program Leg 187 in the Australian Antarctic Discordance, Southeast Indian Ridge (41°–46°S, 126°–135°E) were analyzed, and modeling of the theoretical equilibrium petrogenetic conditions between olivine and melt was conducted. The cores of larger olivine phenocrysts, particularly in the isotopic Indian-type mid-ocean-ridge basalt (MORB), are not equilibrated with melt compositions and are considered to be xenocrystic. Larger plagioclase phenocrysts with compositionally reversed zonation are also xenocrystic. The compositions of primary magma were calculated using a "maximum olivine fractionation" model for primitive MORB that should fractionate only olivine. Olivine compositions equilibrated with calculated primary magma and compositions of calculated primary magma suggest that (1) isotopic Pacific-type MORB is more fractionated than Indian-type MORB, (2) Pacific-type MORB was produced by higher degrees of partial melting than Indian-type MORB, and (3) primary magma for Indian-type MORB was segregated from mantle at 10 kbar (~30 km depth), whereas that for Pacific-type MORB was segregated at 15 kbar (~45 km depth).

[1]Sato, H., 2004. Mineral compositions of MORB from the Australian Antarctic Discordance (AAD): implications for mantle source characteristics. *In* Pedersen, R.B., Christie, D.M., and Miller, D.J. (Eds.), *Proc. ODP, Sci. Results,* 187, 1–26 [Online]. Available from World Wide Web: <http://www-odp.tamu.edu/publications/187_SR/VOLUME/CHAPTERS/202.PDF>. [Cited YYYY-MM-DD]
[2]School of Business Administration/Institute of Natural Science, Shenshu University, 2-1-1 Higashimata, Tama, Kawasaki, Kanagawa 214-8580, Japan.
satohiro@isc.senshu-u.ac.jp

Initial receipt: 17 May 2002
Acceptance: 17 July 2003
Web publication: 17 February 2004
Ms 187SR-202

INTRODUCTION

Mid-ocean-ridge basalt (MORB) erupted along the Indian Ocean spreading center are isotopically distinct from those erupted along the Pacific and Atlantic Ocean spreading centers (Dupré and Allègre, 1983; Hart, 1984). Indian Ocean MORB is characterized by high $^{87}Sr/^{86}Sr$, $^{207}Pb/^{204}Pb$, and $^{208}Pb/^{204}Pb$ for a given value of $^{206}Pb/^{204}Pb$ (e.g., Klein et al., 1988). Within the Australian Antarctic Discordance (AAD), located along the Southeast Indian Ridge (SEIR) south of Australia (Fig. **F1A**), a uniquely sharp isotopic boundary between the Indian Ocean and Pacific Ocean mantle provinces has been recognized (Klein et al., 1988). Based on isotopic analyses of MORB samples dredged from the present spreading axis in the AAD, only basalts younger than 3–4 Ma exhibit Pacific-type isotope signatures (Pyle et al., 1992; Christie et al., 1998). These data form the basis for a hypothesis that proposes rapid westward migration of Pacific mantle during the last 4 m.y. (Christie et al., 1998).

During Ocean Drilling Program (ODP) Leg 187 (Shipboard Scientific Party, 2001), 23 holes were drilled at 13 sites across the hypothesized isotope boundary forming the eastern terminus of the AAD along a swath of 10- to ~30-Ma seafloor interpreted from magnetic anomalies (Fig. **F1B**). Isotope mantle types, Indian, Pacific, and transitional-Pacific, were assigned to basalts collected during Leg 187 based on shipboard geochemical analysis of Ba and Zr contents of basalt glasses of younger lavas from the AAD and east of the AAD (Shipboard Scientific Party, 2001). The following relationships are summarized from the shipboard identifications: (1) there is a plausible mantle province boundary east of the regional residual depth anomaly (difference between the depth of seafloor and that expected from depth-age relations found for other ocean basins: e.g., Marks et al., 1990), and (2) basalts derived from Indian and Pacific mantle types alternate on a timescale of a few million years between 28 and 14 Ma along a flowline in western Zone A (Shipboard Scientific Party, 2001).

In this study, I will report chemical compositions of minerals in basalts collected from the AAD during Leg 187. Complemented with whole-rock major element compositions, I will discuss petrogenetic conditions, particularly pressure (depth) for magma segregation and estimate primary magma compositions for Indian- and Pacific-type MORB.

GEOLOGICAL SETTING AND LOCATION OF ODP SITES

The AAD is a segment of anomalous "chaotic" bathymetry and gravity along the SEIR between 120° and 128°E. Weissel and Hayes (1971) subdivided the SEIR south of Australia into three zones, Zone A (east of the AAD), Zone B (the AAD itself), and Zone C (west of the AAD), based on striking contrasts in seafloor morphology and geophysical data. In spite of a regionally uniform spreading rate (~74 mm/yr full rate), axial morphology between Zone A and Zone B (AAD) is quite different; Zone A exhibits a bathymetry similar to the fast-spreading East Pacific Rise–type spreading axis, whereas Zone B (AAD) has a deeper axial ridge similar to the slow-spreading Mid-Atlantic Ridge (e.g., Palmer et al., 1993; Shipboard Scientific Party, 2001).

F1. Regional map of the SEIR and Leg 187 drill sites, p. 16.

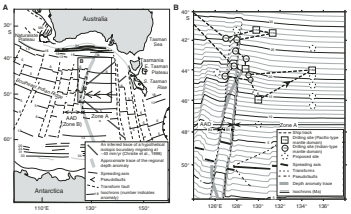

Within the AAD (Zone B), five short but distinct and well-defined segments were denoted as B1–B5 from west to east (Vogt et al., 1983). The isotopic boundary between the Indian Ocean and Pacific Ocean mantle isotopic provinces for zero-age MORB lies within Segment B5 of the AAD (Pyle et al., 1992; Christie et al., 1998). The locality where Pacific-type MORB was recovered in Segment B5 is situated in "normal" seafloor terrain within a west-pointing V-shaped region (Christie et al., 1998). The bathymetric depth anomaly forms a shallow, west-pointing V or U shape, which stretches across the ocean floor from Antarctica to Australia (Marks et al., 1990) (Fig. F1A).

In order to determine the location of the isotopic boundary, 13 sites were drilled during Leg 187: four sites in Segments B4 and B5, six sites in the western part of Zone A, and two sites in central Zone A were chosen for drilling (Fig. F1B). Isotopic domains (Pacific or Indian) used in this study refer to Christie et al. (this volume) rather than shipboard discrimination (Shipboard Scientific Party, 2001). Based on postcruise isotope analysis, samples from Leg 187 are divided into two mantle domains: Pacific-type MORB and Indian-type MORB (Christie et al., this volume).

MINERAL COMPOSITIONS

Analytical technique

Mineral compositions were analyzed on a JEOL JXA-8900R Superprobe equipped with five wavelength-dispersive spectrometers (WDS) at the Ocean Research Institute of the University of Tokyo, Japan. Silicate and oxide minerals were analyzed using a focused beam, an accelerating voltage of 15 kV, and a beam current of 12 nA. To measure NiO contents in olivine, Ni was analyzed with a counting time of 60 s at peak position with 30 s of background measurement. The standard deviation of X-ray counting for NiO analysis in olivine was <10%. Other elements were analyzed with a counting time of 20 s at peak position and 10 s of background measurement. Fe^{2+} and Fe^{3+} contents in spinel were calculated using the method of Droop (1987).

Olivine

Chemical compositions of olivine grains are listed in Table T1 and shown on an NiO vs. Mg# (Mg/[Mg+Fe]×100) diagram (Fig. F2). In general, the centers of phenocrysts (PC) (Table T1) have Mg-rich compositions (Mg# > 80) that are higher than phenocryst peripherals, microphenocrysts, and groundmass olivine grains. However, even groundmass olivine grains (GM) (Table T1) have relatively Mg-rich compositions, generally higher than Mg# ~80 (olivine grains poorest in Mg are found in the groundmass of Sample 187-1154A-2R-1, 46–49 cm; Mg# = 79.81 ± 1.15 [1-σ statistical variation]). Compositional variations of olivine in each sample (at least in each thin section) are very low, and differences of Mg# between PC and GM are <4–5. Olivine grains in Indian-type basalts are generally richer in magnesium than those in Pacific-type basalts.

NiO contents in olivine are also relatively constant, corresponding to restricted variations in Mg#. Central parts of olivine phenocrysts contain 0.2 to 0.3 wt% NiO, and olivine grains in the groundmass contain 0.1 to 0.2 wt% NiO (Fig. F2).

T1. Chemical compositions of olivine grains, p. 24.

F2. Compositions of olivine in lavas, p. 17.

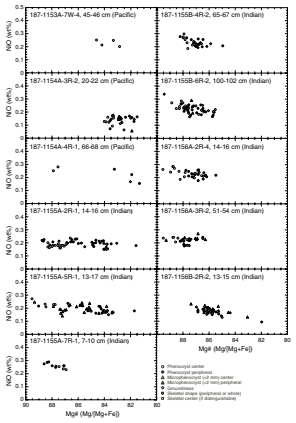

Plagioclase

Chemical compositions of plagioclase grains are listed in a supplementary data file (see the "Supplementary Material" contents list). Because compositional zoning occurs to some extent in plagioclase, compositional variations within plagioclase grains are significantly higher than in olivine grains. In general, the central parts of plagioclase phenocrysts have higher Ca compositions than phenocryst peripherals, microphenocrysts, or groundmass plagioclase. Oscillatory zoning is developed in some large phenocrysts (Fig. F3A), and a few analyzed grains have reversed zoning.

Results of linear compositional profiles for larger plagioclase phenocrysts are shown in Figure F3. In most phenocrysts (with the exception of a few samples with oscillatory zoning patterns), the central parts of phenocrysts have the highest An contents (Fig. F3B) and compositions change abruptly near the peripheral regions of phenocrysts (within ~0.1 mm of the rim). As shown in Figure F3B, phenocryst centers have compositions $\geq An_{80}$ and the peripheral zones of phenocrysts have An_{60-70}. A few grains, particularly in Sample 187-1155A-2R-1, 14–16 cm, have striking reversed zonation compositional patterns. It is noteworthy that plagioclases with both normal (Fig. F3C) and reversed (Fig. F3D) zoning coexist. In Sample 187-1155A-2R-1, 14–16 cm, plagioclase phenocrysts with reversely zoned compositional patterns (Fig. F3D) are larger (1–1.5 mm in size) than those with normal zoning (Fig. F3C) (~0.5 mm in size). Even in reversely zoned plagioclase phenocrysts, peripheral zones (within ~0.1 mm of rim) show normal zoning.

In samples with doleritic texture (Samples 187-1158C-2R-1, 57–60 cm; 187-1161A-4R-1, 116–119 cm; and 187-1162A-5R-1, 0–4 cm), plagioclase compositions are more sodic (commonly $An_{<60}$), particularly for plagioclase grains in the groundmass.

F3. Liner composition of plagioclase phenocrysts, p. 19.

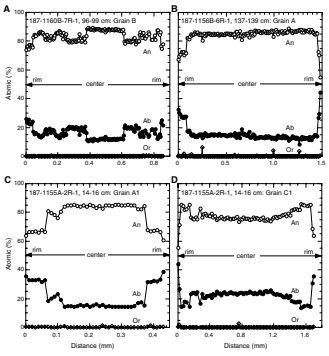

Pyroxene

In most samples, clinopyroxene grains are scattered in an intergranular textural groundmass. Although chemical compositions of pyroxene in the groundmass differ from sample to sample, most grains have Mg# = 70 ~ 80 and $Fs_{10\sim20}En_{40\sim45}Wo_{40\sim45}$ (see the "Supplementary Material" contents list). Only a few grains have subcalcic augite to pigeonite compositions.

Only one basalt sample (Sample 187-1154A-7R-1, 110–113 cm) contains clinopyroxene as both a phenocryst and a microphenocryst. One phenocryst forming a small (~1 mm in size) glomeroporphyritic assemblage with plagioclase has Mg# = 81.7 and $Fs_{11.6}En_{51.9}Wo_{36.5}$ as an average composition. Microphenocrysts have similar compositions to this phenocryst.

Spinel

Only small amounts of spinel are contained in basaltic samples from Leg 187. Chemical compositions are listed in a supplementary data file (see the "Supplementary Material" contents list). $Mg/(Mg+Fe^{2+})$ of spinel ranges from 0.53 to 0.67, and Cr/(Cr+Al) ranges from 0.42 to 0.56. These values resemble previously reported compositional ranges of spinel in MORB (e.g., Dick and Bullen, 1984).

EQUILIBRATED OLIVINE COMPOSITION WITH MELT AND PRIMARY MAGMA COMPOSITION

Calculation of Equilibrated Olivine Compositions

Chemical compositions of primary basaltic magmas beneath the AAD (i.e., magmas equilibrated with the upper mantle) were back calculated from basalt compositions based on the "olivine maximum fractionation" model (e.g., Tatsumi et al., 1983; Yamashita and Tatsumi, 1994; Yamashita et al., 1996; Tamura et al., 2000). In this model, the chemical composition of olivine in equilibrium with basalt was first calculated based on both Fe-Mg and Ni-Mg exchange partitioning between olivine and silicate melt. The calculated olivine composition was then added to the original whole-rock composition in a weight ratio of 1:99, and this was repeated until the equilibrium olivine had an NiO composition equivalent to that of mantle olivine. The olivine composition that was calculated in each step was fractionated from an original primary magma to yield the present basalt composition. Furthermore, whole-rock composition generated by the same number of calculation steps as olivine composition that reached mantle composition represented the melt composition that was finally equilibrated with mantle olivine (i.e., primary magma).

Assumptions involved in the calculation are as follows:

1. $K_d^{Fe\text{-}Mg}{}_{olivine\text{-}melt} = 0.27 + 0.03(N^{MgO}{}_{melt} + 0.33N^{FeO}{}_{melt})$, where N = chemical composition (Takahashi, 1987).
2. $K_d^{Ni\text{-}Mg}{}_{olivine\text{-}melt} = 2.8 - 0.033(N^{MgO}{}_{melt} + 0.33N^{FeO}{}_{melt})$ (Takahashi, 1987).
3. $Fe^{3+}/(Fe^{2+}+Fe^{3+})$ in the melt is kept at 0.05 (Christie et al., 1986).
4. The composition of mantle olivine lies within the "mantle olivine array" (Takahashi, 1987).

This calculation assumes that only olivine was fractionated from magma prior to eruption. If plagioclase was fractionated, the calculation gives an overestimation of the value of MgO in primary magma. On the other hand, if clinopyroxene was fractionated, the calculation gives an underestimation of the value of MgO in primary magma. Therefore, a starting composition that is likely to have only crystallized olivine must be chosen before such a calculation can be performed.

Figure F4 shows major element variation diagrams for basaltic glass from the AAD collected during Leg 187 (C. Russo, unpubl. data). On a CaO/Al_2O_3 vs. MgO diagram (Fig. F4C), CaO/Al_2O_3 values of Pacific-type MORB are scattered, whereas CaO/Al_2O_3 values of Indian-type MORB are relatively constant at >8 wt% MgO and increase at <8 wt% MgO. On an Na_2O vs. MgO diagram (Fig. F4B), Indian-type MORB has relatively constant values at >8 wt% MgO and increases with decreasing MgO; Na_2O increases with decreasing MgO for Pacific-type MORB. The FeO vs. MgO diagram (Fig. F4A) shows similar tendencies as the Na_2O vs. MgO diagram. FeO of Indian-type MORB is relatively constant at >8 wt% MgO, then increases with decreasing MgO; Pacific-type MORB shows a systematic increase in FeO with decreasing MgO.

In accordance with the assertions of Klein and Langmuir (1987), major element variations for Indian-type MORB indicate plagioclase fractionation prior to eruption for basalt with <8 wt% MgO, whereas

F4. Major element diagrams for lava glass, p. 20.

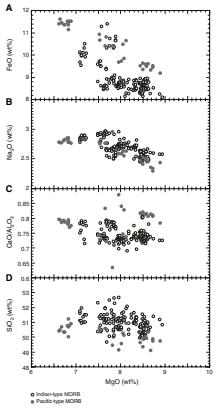

Indian-type MORB with >8 wt% MgO is considered to fractionate only olivine. Therefore, only basalts containing >8 wt% MgO are suitable for calculation of Indian-type MORB based on the olivine maximum fractionation. For Pacific-type MORB, it is concluded that all basalts had fractionated plagioclase. However, rare earth element (REE) chondrite-normalized patterns for Pacific-type MORB reported by C. Russo (unpubl. data) indicate that basalts from Site 1160 have the lowest REE concentrations. Furthermore, basalts from Site 1160 have smaller FeO/MgO (close to 1) and relatively high mg# (= Mg/[Mg+total Fe]) than other Pacific-type MORB (Table T2). These lines of evidence suggest that basalts from Site 1160 are not as highly evolved as other Pacific-type MORB. In this manuscript, the olivine maximum fractionation calculation can be applied to only basalts from Site 1160 for Pacific-type MORB, with the assumption that the effect of fractionation of plagioclase is lowest for these samples. It should be recognized that any estimates of primary MgO contents for these samples are slightly overestimated.

Based on the criteria mentioned above and proximity of analyzed samples in this study and Shipboard Scientific Party (2001) and/or C. Russo (unpubl. data), five samples were chosen from Indian-type MORB and two samples were chosen from Pacific-type MORB as starting compositions for the calculations. Each chosen sample belongs to the same lithologic unit as that containing the analyzed olivine grains. The chemical compositions of these samples are listed in Table T2.

T2. Whole-rock and/or glass compositions for calculations, p. 25.

"Actual" Olivine Compositions vs. Calculated Olivine Compositions

Figure F5 shows Mg#-NiO plots of analyzed "actual" olivine composition (phenocryst center/peripheral, microphenocryst center/peripheral, and groundmass grains) for selected basalt samples. Also shown in each diagram is the Mg#-NiO variation for mantle olivine (mantle olivine array) as well as the "back-calculated" trend of calculated "equilibrium" olivine compositions. If the olivine phenocrysts in a given basalt represent crystals that crystallized from a melt of the same composition as a given basalt, they should coincide with the low-Mg# end of the back-calculated trend. This appears to be the case for Pacific-type MORB, whereas it clearly not the case for most of Indian-type MORB, which contains many olivine crystals that have more magnesian compositions than expected. In particular, Sample 187-1155A-5R-1, 13–17 cm, exhibits a significant disequilibrium between actual olivine phenocrysts and calculated olivine compositions. This disequilibrium could be due to (1) precision of shipboard whole-rock analysis, (2) whole-rock compositions that are not representative of the bulk composition of the lava, or (3) another origin for phenocrysts. Whole-rock composition for Sample 187-1155A-5R-1, 20–23 cm, was analyzed by the inductively coupled plasma–atomic emission spectrophotometer (ICP-AES) on the *JOIDES Resolution* during Leg 187. Because the total composition for Sample 187-1155A-5R-1, 20–23 cm, exceeds 100 wt% (102.20 wt%) (Shipboard Scientific Party, 2001), the problem of accuracy during analysis still remains. However, the difference between actual olivine phenocrysts and calculated olivine compositions is too large to be explained solely by analytical precision. Because of rapid quenching of the margins, flow differentiation, crystal setting, and many other factors, small subsamples taken from different parts of the lava flow can have very different compositions. It is very difficult to determine what

F5. NiO vs. Mg# for "actual" and calculated olivine, p. 21.

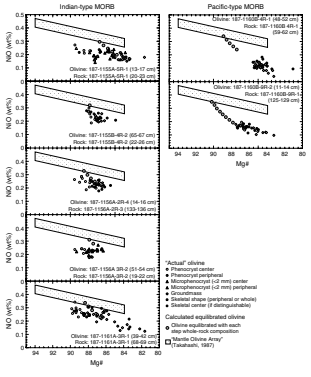

part of the flow was sampled during Leg 187 because of low recovery. Therefore, although samples for whole-rock analysis belong to the same lithologic unit as that containing the analyzed olivine grains, it is plausible that they do not completely have the same compositions. Basalts from other sections of Hole 1155A (187-1155A-2R-1, 14–16 cm) have larger plagioclase phenocrysts with compositionally reversed zoning. Relatively smaller and abundant plagioclase phenocrysts have normal compositional zoning. Therefore, larger plagioclase phenocrysts in basalts (Sample 187-1155A-2R-1, 14–16 cm) are considered to be xenocrystic. Large olivine and plagioclase phenocrysts form glomeroporphyritic assemblages in Sample 187-1155A-2R-1, 14–16 cm. Thus, the olivine phenocrysts are also considered to be xenocrysts. Compositional variation in olivine grains in Sample 187-1155A-2R-1, 14–16 cm, is very similar to that in Sample 5R-1, 20–23 cm, suggesting that olivine phenocrysts in the latter sample, are also xenocrysts. These observations may explain disequilibrium between "real" and calculated olivine compositions in Indian-type MORB, suggesting that many of the Mg-rich olivine phenocrysts in Indian-type MORB are, in fact, xenocrysts.

Because the length of the back-calculated trend indicates the extent of olivine fractionation from an original primary magma required to produce a given basalt, Pacific-type MORB has undergone much more extensive preeruption fractionation than Indian-type MORB. For Indian-type MORB, calculated olivine compositions reach the "mantle olivine array" after zero to four steps of calculation, whereas four to seven steps are needed for Pacific-type MORB. Groundmass olivine grains of Sample 187-1160B-4R-1, 48–52 cm, have different compositions from calculated olivine equilibrated with melt at the final stage of fractionation. This disequilibrium can be explained if crystallized olivine phenocrysts and/or microphenocrysts with compositions of $Fo_{85–87}$ were removed from the magma just before eruption.

Primary Magma Compositions

The diagrams in Figure **F5** can be used to estimate the major element composition of the original, prefractionation, primary melt for each basalt as mentioned above. Compositions of the estimated primary melt and olivine equilibrated with mantle are listed in Table **T3.** Although differences in olivine compositions between Indian- and Pacific-type MORB are small, olivine compositions calculated for Indian-type MORB have lower Mg# and NiO contents (86.8 ~ 88.5 and 0.296 ~ 0.339, respectively) than those calculated for Pacific-type MORB (88.9 ~ 90.2 and 0.342 ~ 0.351, respectively).

Estimated primary magma compositions for both Indian- and Pacific-type MORB were plotted on an olivine-plagioclase-quartz (Ol-Pl-Qz [silica]) diagram of Walker et al. (1979) overlain with the isobaric liquid compositional trend of lherzolite determined by Hirose and Kushiro (1993) (Fig. **F6**). The locations of these primary magmas in Figure **F6** are considered to represent the pressure (i.e., depth) where melt was fully equilibrated with mantle material or where melt was produced. Calculated compositions of primary magma in this study indicate that Indian-type MORB was equilibrated with mantle materials (or was produced) at pressures of ~10 kbar (~30 km depth), whereas Pacific-type MORB was equilibrated at ~15 kbar (~45 km depth).

T3. Compositions of primary melts and equilibrated olivine, p. 26.

F6. Olivine-plagioclase-silica projection, p. 22.

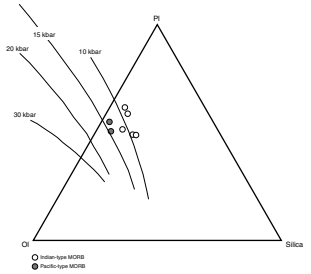

DISCUSSION

Previous geochemical studies reveal that two isotopically distinct mantle sources underlie the SEIR between Australia and Antarctica (e.g., Pyle at al., 1992; Christie et al., 1998). During ODP Leg 187 older oceanic crusts off axis of the AAD were drilled, and chemical analysis of sampled material shows that an isotopic boundary has existed there since at least ~30 Ma, with small-scale perturbations in timescale and in space (Shipboard Scientific Party, 2001). It is plausible that the Indian/Pacific isotopic boundary has slowly migrated westward, as opposed to the rapid-migration hypothesis suggested by Christie et al. (1998) based on geochemical results from ODP Leg 187 (see other chapters in this volume). Therefore, petrogenetic conditions inferred from petrological data should also reflect the essential differences between Indian and Pacific MORB sources.

Compositions of estimated primary magma indicate the depth of melt segregation from the surrounding mantle material. The compositions calculated in this study indicate that the depth for Indian-type MORB is shallower than that for Pacific-type MORB if compositions of source mantle do not differ significantly. Potassium components in mantle peridotites will lower the solidus temperature (Takahashi and Kushiro, 1983), and increased potassium and sodium components will shift the isobaric liquid compositional trend toward the silica apex on a CIPW norm projection (Sweeney et al., 1991). However, contents of potassium and sodium (or NaK# by Sweeney et al., 1991) are not significantly different between the two types of MORB analyzed here. Therefore, the calculated difference in the depth of melt segregation of Pacific-type and Indian-type MORB is realistic, although the absolute values of these depths may indicate a shallower limit of the depth.

Previous petrological studies reported that the AAD lavas have higher MgO contents and higher $Na_{8.0}$, lower $Fe_{8.0}$, and higher $Si_{8.0}$ values than Zone A lavas (i.e., Pacific-type MORB), indicating lower degrees of partial melting and lower mean pressures of melting beneath the AAD (Klein et al., 1991). Compositions of glass samples from Leg 187 confirm this relationship (C. Russo, unpubl. data) (Fig. **F4**). Figure **F7** illustrates a schematic model for petrogenetic conditions beneath the AAD, and details of the model including the previous results are described below. Beneath Zone A, the onset of partial melting starts and segregation of melt from mantle material occur at deeper level than beneath the AAD. Because the degree of partial melting for Indian-type MORB is lower than Pacific-type MORB, the hypothetical melting column beneath the AAD (Indian-type mantle) is shorter than that beneath Zone A (Pacific-type mantle).

F7. Model for petrogenetic conditions at the AAD, p. 23.

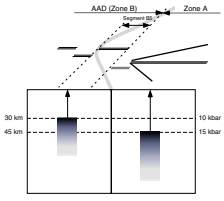

Calculated olivine composition equilibrated with primary magma for the Indian-type MORB has a slightly Fe-richer composition (Mg# = 86.8–88.5) than that for Pacific-type MORB (88.9–90.2), indicating the heterogeneity of the MORB source. According to Ozawa (1997), the "mantle olivine array" includes two distinct origins of olivine in mantle. One is due to partial melting of original mantle peridotite. In this case, residual olivine occupies a high-Mg# portion (Mg# > 90) of the mantle olivine array. Another origin of the mantle olivine array is related to interaction between high Mg#–high NiO olivine in mantle peridotite and melt that is equilibrated with low Mg#–low NiO olivine. This interaction produces olivine that has a composition at a low-Mg# portion (Mg# < 90) of the mantle olivine array. Because primary magma for

Indian-type MORB appears to be equilibrated with low-Mg# olivine, it is plausible that the Indian-type MORB source consists of mixture of mantle peridotite and material derived from melt that is equilibrated with low Mg#–NiO olivine. On the other hand, primary magma for Pacific-type MORB was equilibrated with residual mantle olivine by partial melting. Therefore, in terms of petrogenetic conditions inferred by mineral compositions and whole-rock major element composition, it is suggested that differences between the Indian- and Pacific-type MORB from around the AAD result from mantle source compositions.

CONCLUSIONS

Minerals in MORB samples from the AAD along the SEIR were analyzed, and the following conclusions were obtained.

1. Olivine phenocrysts and even olivine grains in the groundmass are rich in Mg (Mg# > 80). Olivine phenocryst centers contain up to 0.3 wt% NiO, whereas olivine grains in the groundmass contain up to 0.2 wt% NiO.
2. Olivine fractional crystallization pathways were calculated for primitive MORB samples, five samples for Indian-type MORB and two samples for Pacific-type MORB. During this calculation, olivine compositions equilibrated with melt composition were calculated. Compositions of olivine phenocrysts in some Indian-type MORB are not equilibrated with those of the calculated olivine. Precision of whole-rock analysis, sampling bias in lava flow, or xenocrystic origin were considered to explain the disequilibrium. In these samples, large plagioclase phenocrysts show reversed compositional zoning. It is plausible that these phenocrysts are xenocrystic.
3. The number of calculation steps required to equilibrate olivine compositions to mantle olivine composition (i.e., degree of fractionation) suggests that Pacific-type MORB is more fractionated than Indian-type MORB.
4. Estimated compositions of primary magma determined by the olivine fractionation calculation were compared to previously reported results from experimental petrology, and the results of this comparison suggest that Indian-type MORB segregated from mantle material at 10 kbar (~30 km depth), whereas Pacific-type MORB segregated at 15 kbar (~45 km depth).
5. Olivine equilibrated with Pacific primary magma has Mg# = ~90, whereas olivine equilibrated with Indian primary magma has Mg# = 86.8–88.5. Composition of equilibrated olivine with calculated primary magma suggests that the mantle source for Indian-type MORB was mixture of mantle peridotite and material derived from melt equilibrated with low Mg#–low NiO olivine.

ACKNOWLEDGMENTS

This research used samples and/or data provided by the Ocean Drilling Program (ODP). ODP is sponsored by the U.S. National Science Foundation (NSF) and participating countries under management of Joint Oceanographic Institutions (JOI), Inc.

Discussions with David Christie and Paul Wallace during the post-cruise meeting are much appreciated. Daniel Curewitz provided critical comments and a fruitful review on earlier versions of this manuscript. Discussions with Teruaki Ishii and Hidetsugu Taniguchi were very fruitful. The manuscript was reviewed and revised by James Brophy, Pat Castillo, and Jay Miller, to whom the author is grateful. Thanks are also due to Naoko Suyeda, who prepared most of the thin sections analyzed in this study.

REFERENCES

Christie, D.M., Carmichael, I.S.E., and Langmuir, C.H., 1986. Oxidation states of mid-ocean ridge basalt glasses. *Earth Planet. Sci. Lett.,* 79:397–411.

Christie, D.M., West, B.P., Pyle, D.G., and Hanan, B.B., 1998. Chaotic topography, mantle flow and mantle migration in the Australian-Antarctic Discordance. *Nature,* 394:637–644.

Dick, H.J.B., and Bullen, T., 1984. Chromian spinel as a petrogenetic indicator in abyssal and alpine-type peridotites and spatially associated lavas. *Contrib. Mineral. Petrol.,* 86:54–76.

Droop, G.T.R., 1987. A general equation for estimating Fe^{3+} concentrations in ferromagnesian silicates and oxides from microprobe analyses, using stoichiometric criteria. *Mineral. Mag.,* 51:431–435.

Dupré, B., and Allègre, C.J., 1983. Pb-Sr isotope variation in Indian Ocean basalts and mixing phenomena. *Nature,* 303:142–146.

Hart, S.R., 1984. A large-scale isotope anomaly in the Southern Hemisphere mantle. *Nature,* 309:753–757.

Hirose, K., and Kushiro, I., 1993. Partial melting of dry peridotites at high pressures: determination of compositions of melts segregated from peridotite using aggregates of diamond. *Earth Planet. Sci. Lett.,* 114:477–489.

Klein, E.M., and Langmuir, C.H., 1987. Global correlations of ocean ridge basalt chemistry with axial depth and crustal thickness. *J. Geophys. Res.,* 92:8089–8115.

Klein, E.M., Langmuir, C.H., and Staudigel, H.S., 1991. Geochemistry of basalts from the SE Indian Ridge, 115°–138°. *J. Geophys. Res.,* 96:2089–2108.

Klein, E.M., Langmuir, C.H., Zindler, A., Staudigel, H., and Hamelin, B., 1988. Isotope evidence of a mantle convection boundary at the Australian-Antarctic Discordance. *Nature,* 333:623–629.

Marks, K.M., Vogt, P.R., and Hall, S.A., 1990. Residual depth anomalies and the origin of the Australian-Antarctic Discordance Zone. *J. Geophys. Res.,* 95:17325–17337.

Ozawa, K., 1997. Mechanism of magma generation constrained by mantle peridotites: solid-dominant open magma system. *Bull. Volcanol. Soc. Jpn., 2nd Ser.,* 42:S61–S85. (Japanese with English abstract)

Palmer, J., Sempéré, J.-C., Christie, D.M., and Phipps-Morgan, J., 1993. Morphology and tectonics of the Australian-Antarctic Discordance between 123°E and 128°E. *Mar. Geophys. Res.,* 15:121–152.

Pyle, D.G., Christie, D.M., and Mahoney, J.J., 1992. Resolving an isotopic boundary within the Australian-Antarctic Discordance. *Earth Planet. Sci. Lett.,* 112:161–178.

Pyle, D.G., Christie, D.M., Mahoney, J.J., and Duncan, R.A., 1995. Geochemistry and geochronology of ancient southeast Indian and southwest Pacific seafloor. *J. Geophys. Res.,* 100:22261–22282.

Shipboard Scientific Party, 2001. Leg 187 summary. *In* Christie, D.M., Pedersen, R.B., Miller, D.J., et al., *Proc. ODP, Init. Repts.,* 187: College Station TX (Ocean Drilling Program), 1–49.

Sweeney, R.J., Falloon, T.J., Green, D.H., and Tatsumi, Y., 1991. The mantle origins of Karoo picrites. *Earth Planet. Sci. Lett.,* 107:256–271.

Takahashi, E., 1987. Origin of basaltic magmas—implications from peridotite melting experiments and an olivine fractionation model. *Bull. Volcanol. Soc. Jpn., 2nd Ser.,* 30:S17–S40. (in Japanese with English abstract)

Takahashi, E., and Kushiro, I., 1983. Melting of a dry peridotite at high pressures and basalt magma genesis. *Am. Mineral.,* 68:859–879.

Tamura, Y., Yuhara, M., and Ishii, T., 2000. Primary arc basalts from Daisen Volcano, Japan: equilibrium crystal fractionation versus disequilibrium fractionation during supercooling. *J. Petrol.,* 41:431–448.

Tatsumi, Y., Sakuyama, M., Fukuyama, H., and Kushiro, I., 1983. Generation of arc basalt magmas and thermal structure of the mantle wedge in subduction zones. *J. Geophys. Res.,* 88:5815–5825.

Vogt, P.R., Cherkis, N.Z., and Morgan, G.A., 1983. Project investigator–1. Evolution of the Australian-Antarctic Discordance from a detailed aeromagnetic study. *In* Oliver, R.L., James, P.R., and Jago, J.B. (Eds.), *Antarctic Earth Science.* Proc. 4th Int. Symp. Antarct. Earth Sci., 608–613.

Walker, D., Shibata, T., and Delong, S.E., 1979. Abyssal tholeiites from the Oceanographer Fracture Zone, II. Phase equilibria and mixing. *Contrib. Mineral. Petrol.,* 70:111–125.

Weissel, J.K., and Hayes, D.E., 1971. Asymmetric seafloor spreading south of Australia. *Nature,* 231:518–522.

Yamashita, S., and Tastumi, Y., 1994. Thermal and geochemical evolution of the mantle wedge in the Northeast Japan arc, 2. Contribution from geochemistry. *J. Geophys. Res.,* 99:22285–22293.

Yamashita, S., Tatsumi, Y., and Nohda, S., 1996. Temporal variation in primary magma compositions in the Northeast Japan arc. *Isl. Arc,* 5:276–288.

APPENDIX

Petrographic Descriptions

Detailed descriptions of core samples recovered during Leg 187 are reported by the Shipboard Scientific Party (2001). In this appendix, I describe petrographic characteristics of lava samples from Leg 187 used in this research. Sample characteristics are as follows:

187-1153A-7W-4, 45–46 cm: Aphyric lava containing only trace amounts of olivine and plagioclase crystals.

187-1154A-2R-1, 46–49 cm: Olivine-plagioclase porphyritic lava. Groundmass exhibits an intersertal to intergranular texture.

187-1154A-3R-2, 20–22 cm: Olivine-plagioclase glomeroporphyritic lava. Groundmass exhibits an intersertal to intergranular texture. Olivine grains exceed 2.5 mm in diameter in places.

187-1154A-4R-1, 66–68 cm: Clinopyroxene-olivine-plagioclase porphyritic lava. Groundmass exhibits an intersertal to intergranular texture. Oscillatory zoning in plagioclase is well defined.

187-1154A-7R-1, 110–113 cm: Olivine-plagioclase porphyritic lava. Some occurrence of olivine-plagioclase glomerocrysts. Groundmass exhibits an intersertal to intergranular texture.

187-1155A-2R-1, 14–16 cm: Olivine-plagioclase seriatic lava. Groundmass exhibits intersertal texture. Olivine and plagioclase exhibit a small (0.7–1 mm diameter) subpoikilitic glomeroporphyritic texture in places. Larger plagioclase porphyroclasts (1–2 mm in size) exhibit remarkably well defined oscillatory zonings.

187-1155A-5R-1, 13–17 cm: Olivine-plagioclase seriatic lava. Small-scale glomeroporphyritic textures consisting of olivine and plagioclase are observed in places. Subpoikilitic relationships between these two minerals are observed in some cases. Groundmass exhibits an intersertal texture.

187-1155A-7R-1, 7–10 cm: Plagioclase glomeroporphyritic lava. Small amounts of olivine are contained in the glomerocrysts. Groundmass exhibits an intergranular texture of plagioclase and clinopyroxene. Glomeroporphyritic plagioclase >2 mm in diameter in places.

187-1155B-4R-2, 65–67 cm: Olivine-plagioclase glomeroporphyritic lava. Glomeroporphyritic assemblages are >3 mm in diameter in places. Groundmass exhibits an intersertal texture.

187-1155B-6R-2, 100–102 cm: Olivine-plagioclase glomeroporphyritic lava. Some of the larger plagioclase porphyroclasts exhibit oscillatory zoning. Some olivine phenocrysts exhibit euhedral shapes.

187-1156A-2R-4, 14–16 cm: Olivine-plagioclase porphyritic lava. Groundmass exhibits intersertal to intergranular texture. Plagioclase (and olivine) glomeroporphyritic assemblages are scattered throughout the sample. Olivine grains have relatively euhedral shapes. Spinel grains occur as phenocrysts (up to 0.5 mm in diameter) associated with olivine and/or small spinels and are scattered throughout the groundmass.

187-1156A-3R-2, 51–54 cm: Olivine-plagioclase glomeroporphyritic lava. Some larger plagioclase porphyroclasts exhibit oscillatory zoning. Olivine phenocrysts exhibit euhedral to subhedral shapes. Groundmass is partly altered glass and has a hyalophitic texture.

187-1156B-2R-2, 13–15 cm: Olivine-plagioclase seriatic lava. Olivine phenocrysts are usually smaller (<0.5 mm in diameter) than plagioclase phenocrysts (1–2 mm in diameter). Small numbers of small spinel grains occur associated with plagioclase glomeroporphyritic assemblages.

187-1156B-6R-1, 137–139 cm: Olivine-plagioclase porphyritic lava. Olivine and plagioclase occur in glomeroporphyritic assemblages in places. Groundmass exhibits an intersertal texture. Small spinel grains are associated with olivine phenocrysts.

187-1157A-2R-1, 60–64 cm: Olivine-plagioclase porphyritic lava. Plagioclase grains occur as glomeroporphyritic assemblages in places. Larger plagioclase phenocrysts exhibit oscillatory zoning. Groundmass is mostly glassy and has a hyalophitic texture.

187-1157A-3R-2, 12–15 cm: Olivine-plagioclase porphyric lava. Some olivine grains exhibit skeletal shapes. Plagioclase and olivine grains form glomeroporphyritic assemblages in places. Groundmass is glassy and has an intersertal texture.

187-1157B-6R-1, 130–133 cm: Olivine-plagioclase porphyritic lava. Some olivine grains have skeletal shapes. Subpoikilitic relations between olivine and plagioclase in glomeroporphyritic assemblages are observed. Groundmass has an intersertal texture.

187-1158B-4R-1, 88–91 cm: Fine-grained olivine (~0.2 mm in diameter) and plagioclase (~0.5 mm in diameter) microphyric lava. Groundmass has an intersertal to intergranular texture.

187-1158C-2R-1, 57–60 cm: Fine-grained (~0.5 mm in diameter) clinopyroxene-plagioclase subophitic lava. Glass and/or its altered products and opaque minerals (titanomagnetite) occupy interstitial areas.

187-1160B-4R-1, 48–52 cm: Aphyric holocrystalline lava. Fine-grained (<0.3 mm in diameter) olivine, clinopyroxene, and plagioclase are observed.

187-1160B-7R-1, 96–99 cm: Olivine-plagioclase porphyritic lava. Olivine and plagioclase glomeroporphyritic assemblages are observed. Groundmass has an intergranular texture, consisting of

olivine, plagioclase, clinopyroxene, and trace amounts of spinel. Larger plagioclase grains exhibit oscillatory zoning.

187-1160B-7R-2, 14–16 cm: Olivine-plagioclase porphyritic lava. Olivine and plagioclase glomeroporphyritic assemblages are observed. Groundmass has an intergranular texture, consisting of olivine, plagioclase, and clinopyroxene. Small numbers of spinel grains occur as inclusions in the plagioclase phenocryst.

187-1160B-9R-2, 11–14 cm: Olivine-plagioclase porphyritic lava. Some plagioclase grains form glomeroporphyritic assemblages. Groundmass exhibits an intergranular texture, consisting of olivine, plagioclase, and pyroxene.

187-1160B-9R-3, 29–32 cm: Aphyric holocrystalline lava. Fine-grained (<0.3 mm in diameter) clinopyroxene and plagioclase grains with small-scale subophitic textures are observed.

187-1161A-3R-1, 39–42 cm: Olivine-plagioclase porphyritic lava. Olivine and plagioclase grains form glomeroporphyritic assemblages with subpoikilitic texture in places. Small numbers of spinel grains are scattered in groundmass. Groundmass exhibits intersertal texture.

187-1161A-4R-1, 116–119 cm: Sparsely plagioclase porphyritic lava. Plagioclase phenocrysts commonly have oscillatory zoning. Groundmass has subophitic texture with small amounts of glassy material.

187-1161B-1W-1, 44–47 cm: Olivine-plagioclase porphyritic lava. Olivine and plagioclase grains form glomeroporphyritic assemblages in places. Groundmass is mostly glassy and has hyalophitic texture.

187-1162A-5R-1, 0–4 cm: Medium-grained (>1 mm diameter) equigranular plagioclase gabbroic rocks. Plagioclase grains are fresh, but mafic minerals (olivine and clinopyroxene) are commonly altered into oxide mineral, actinolite, and/or chlorite.

187-1164A-3R-1, 45–49 cm: Plagioclase porphyritic lava. Small numbers of olivine grains occur as microphenocrysts. Groundmass has an intergranular to intersertal texture, consisting of olivine, plagioclase, and clinopyroxene.

187-1164B-8R-1, 73–75 cm: Olivine-plagioclase porphyritic lava. Small (~0.5 mm diameter) plagioclase and olivine grains form glomeroporphyritic assemblages in places. Some olivine grains have skeletal shapes. Groundmass is glassy and has a hyalophitic to intersertal texture, consisting of olivine and plagioclase.

187-1164B-9R-1, 59–61 cm: Olivine-plagioclase porphyritic lava. Some olivine grains have skeletal shapes. Groundmass is glassy and has a hyalophitic to intersertal texture, consisting of olivine and plagioclase.

Figure F1. A. Regional map of the Southeast Indian Ocean (modified after Pyle et al., 1995), showing magnetic anomaly (numbers) and Australian Antarctic Discordance (AAD) along the Southeast Indian Ridge. The thin dark V shape east of the AAD indicates an inferred trace of a hypothetical isotopic boundary migrating at ~40 mm/yr (see Christie et al., 1998, for details). Broader gray-colored V shape indicates an approximate trace of the depth anomaly. **B.** Drill sites during ODP Leg 187 (modified after Shipboard Scientific Party, 2001) with seafloor isochrons.

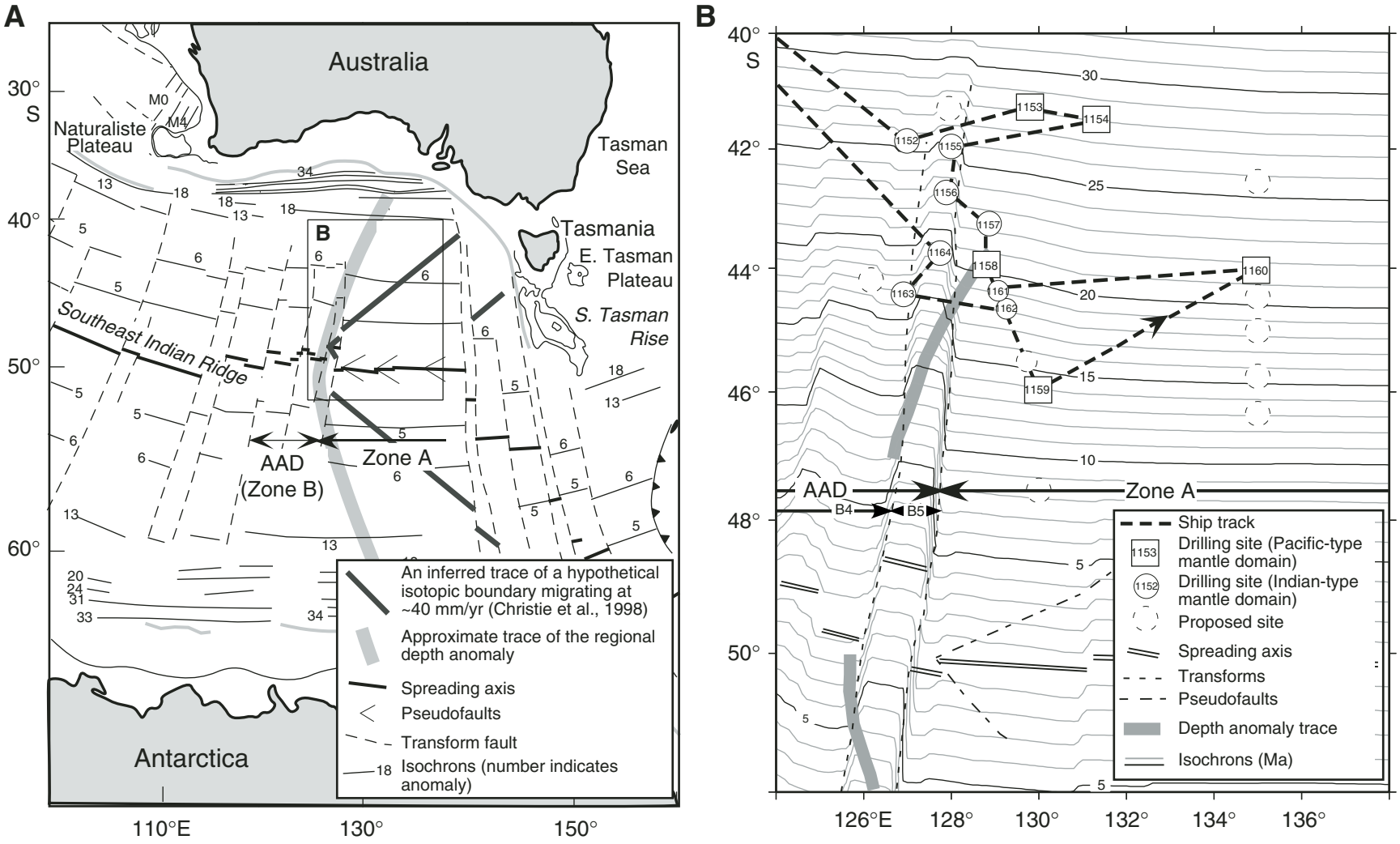

Figure F2. Chemical compositions of olivine in lavas recovered from the AAD during ODP Leg 187 on NiO vs. Mg# (= Mg/[Mg+Fe]×100) diagram. "Indian" and "Pacific" after sample number indicate isotopic mantle province defined by **Christie et al.** (this volume). Continued on next page.

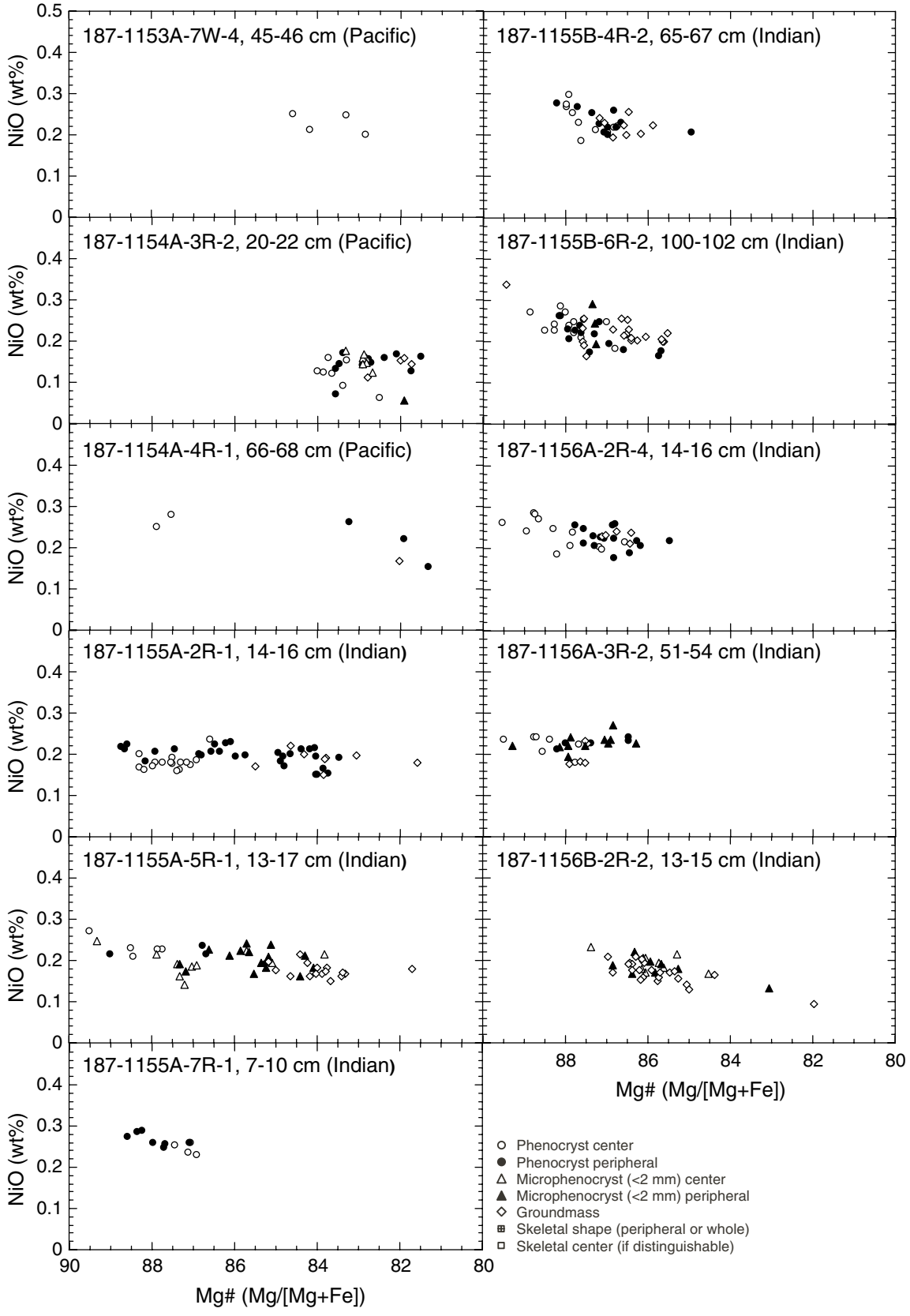

Figure F2 (continued).

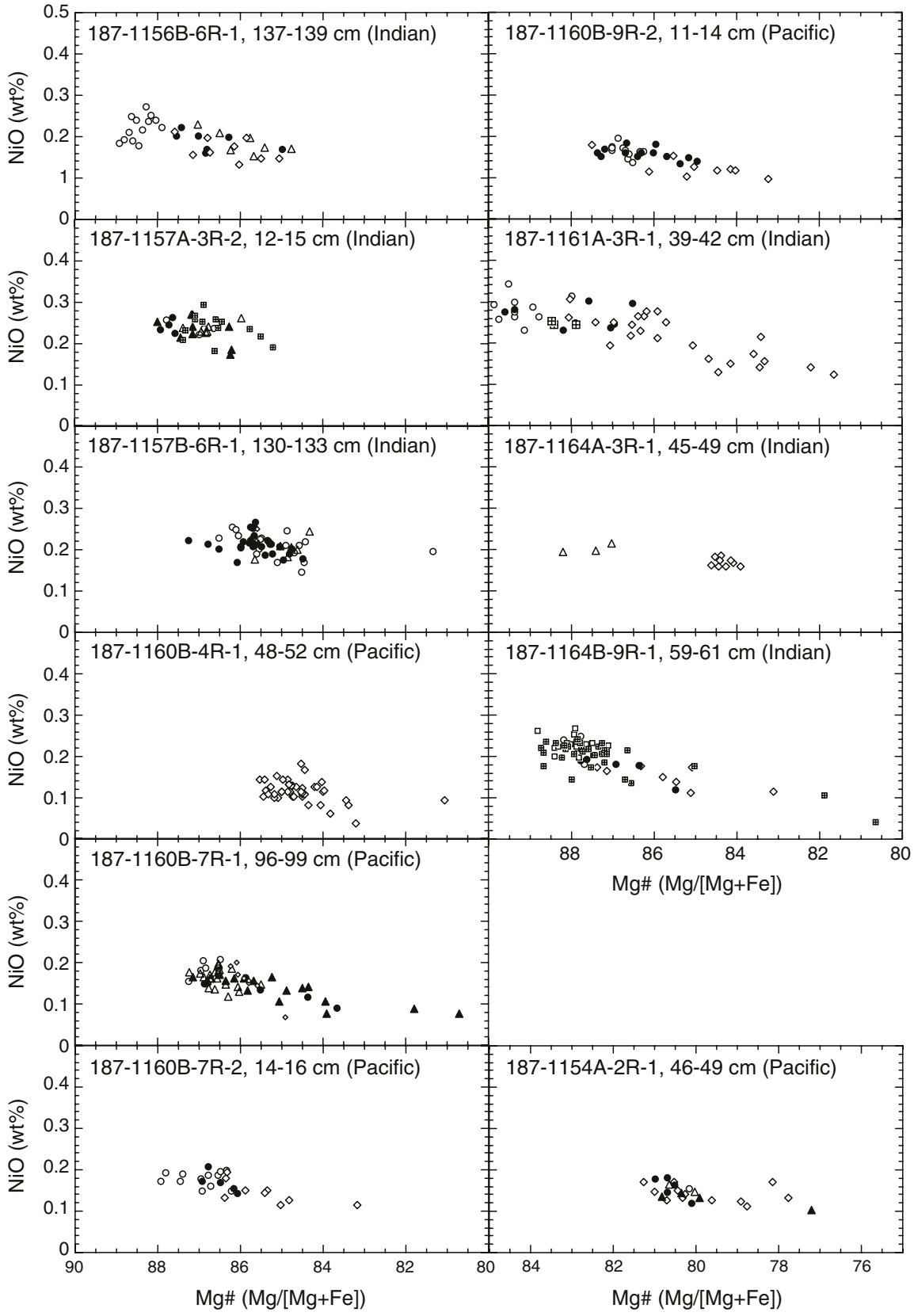

Figure F3. Representative liner compositional profiles of plagioclase phenocrysts in lavas recovered from the AAD during ODP Leg 187. **A, B.** Plagioclase phenocrysts in Pacific-type MORB. **C, D.** Plagioclase phenocrysts in Indian-type MORB. An = anorthite, Ab = albite, Or = orthoclase.

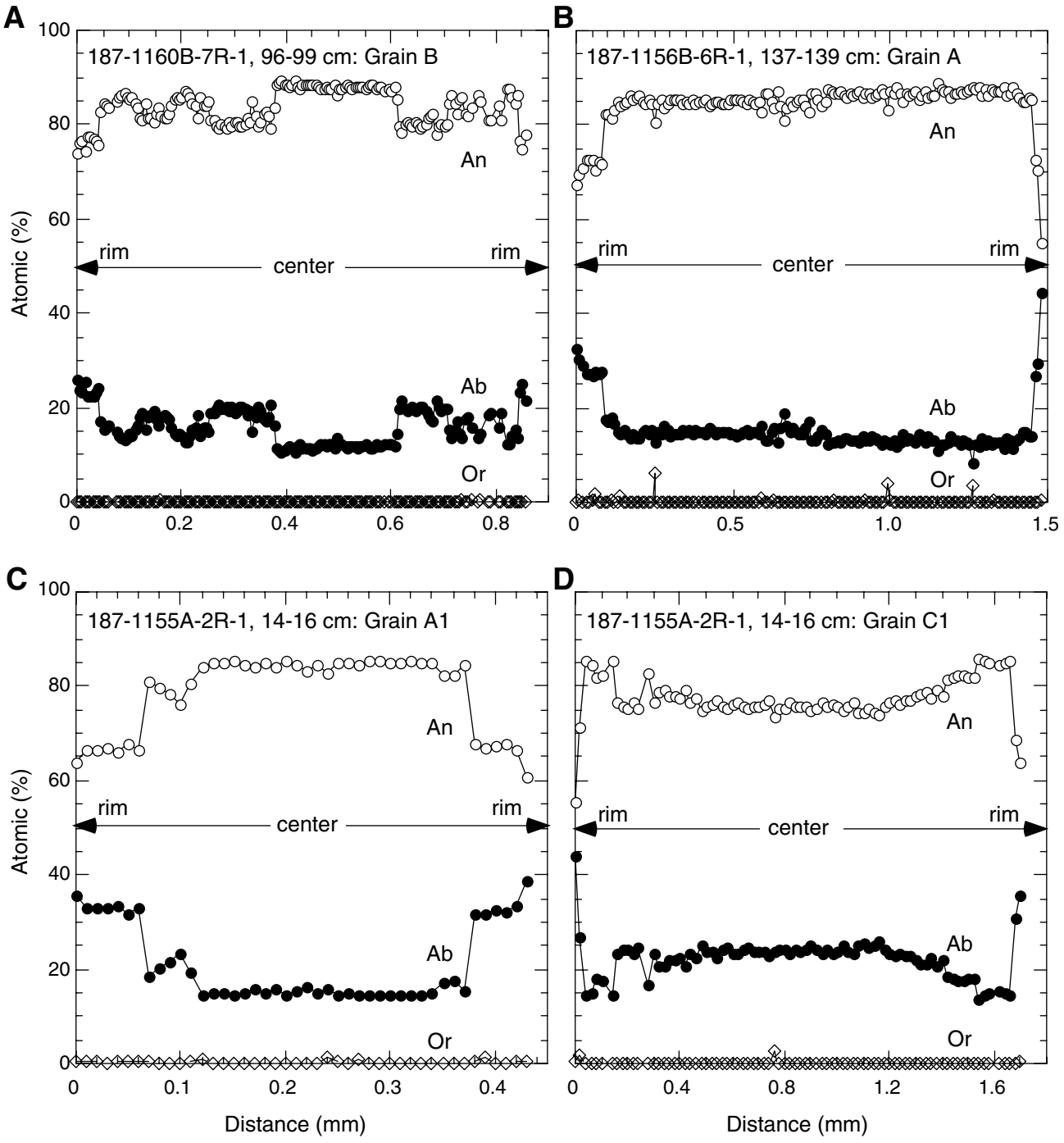

Figure F4. Major element variation diagrams for glass of lavas recovered from the AAD during ODP Leg 187. Data source: C. Russo (unpubl. data). **A.** FeO vs. MgO. **B.** Na_2O vs. MgO. **C.** CaO/Al_2O_3 vs. MgO. **D.** SiO_2 vs. MgO.

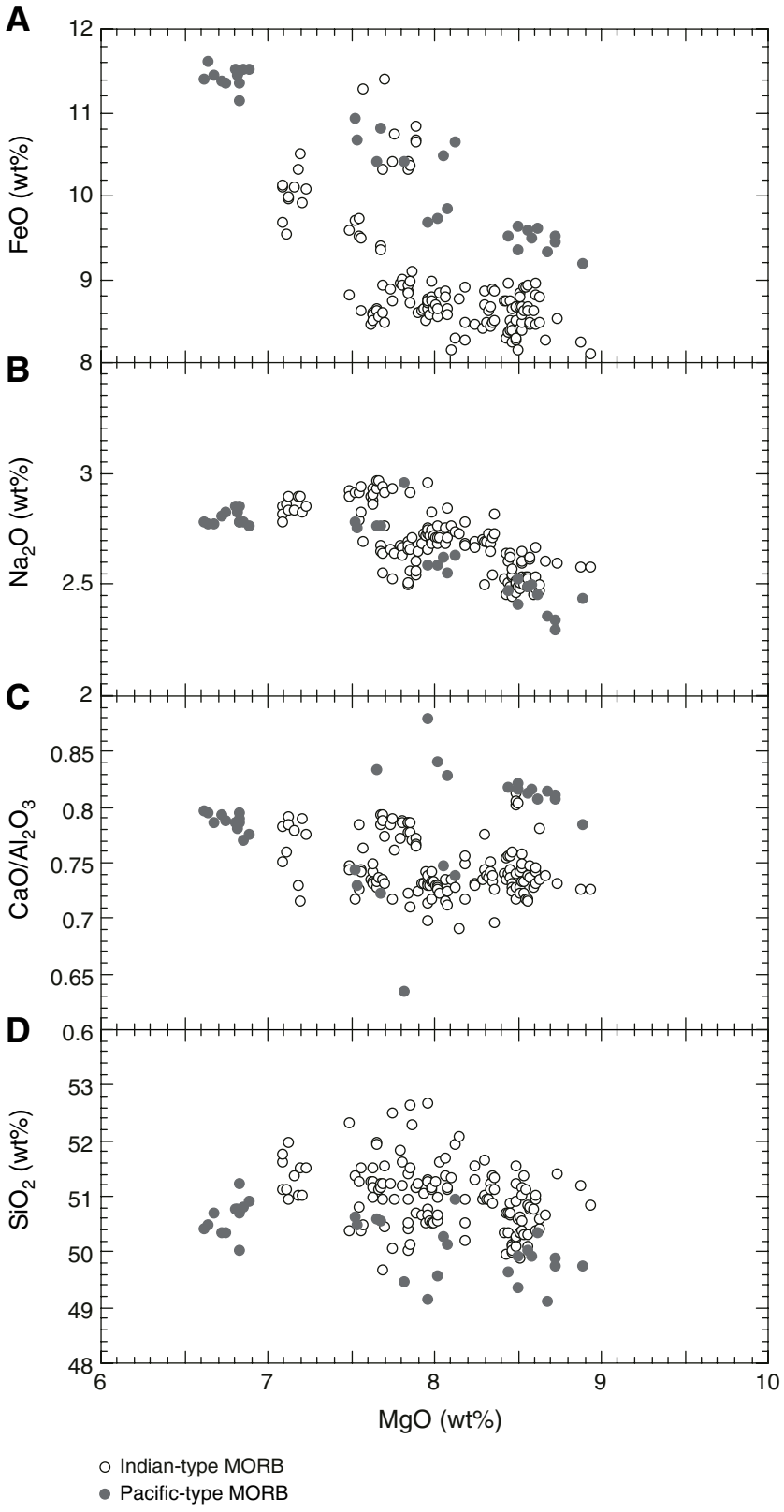

Figure F5. Plots of NiO vs. Mg# for "actual" analyzed olivine (same as Fig. F2, p. 17) and calculated olivine equilibrated with melt. Compositions of olivine equilibrated with melt were calculated by the "olivine maximum fractionation" method as described in the text.

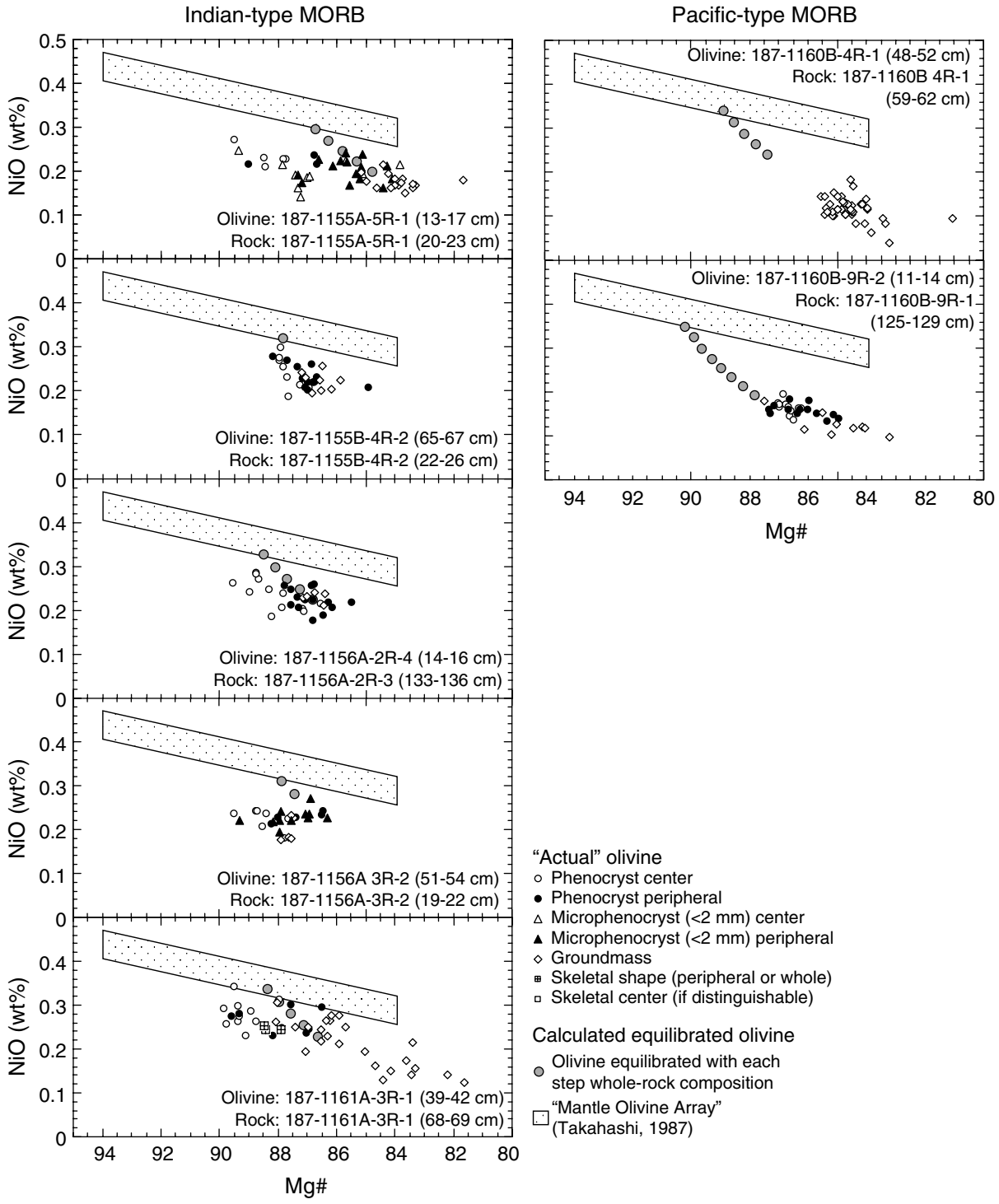

Figure F6. Ol (olivine)-Pl (plagioclase)-Silica (SiO_2) projection of Walker et al. (1979), showing assumed primary magma for lava from the AAD with isobaric liquid compositional trends for dry peridotites (KLB-1 and HK66) by Hirose and Kushiro (1993).

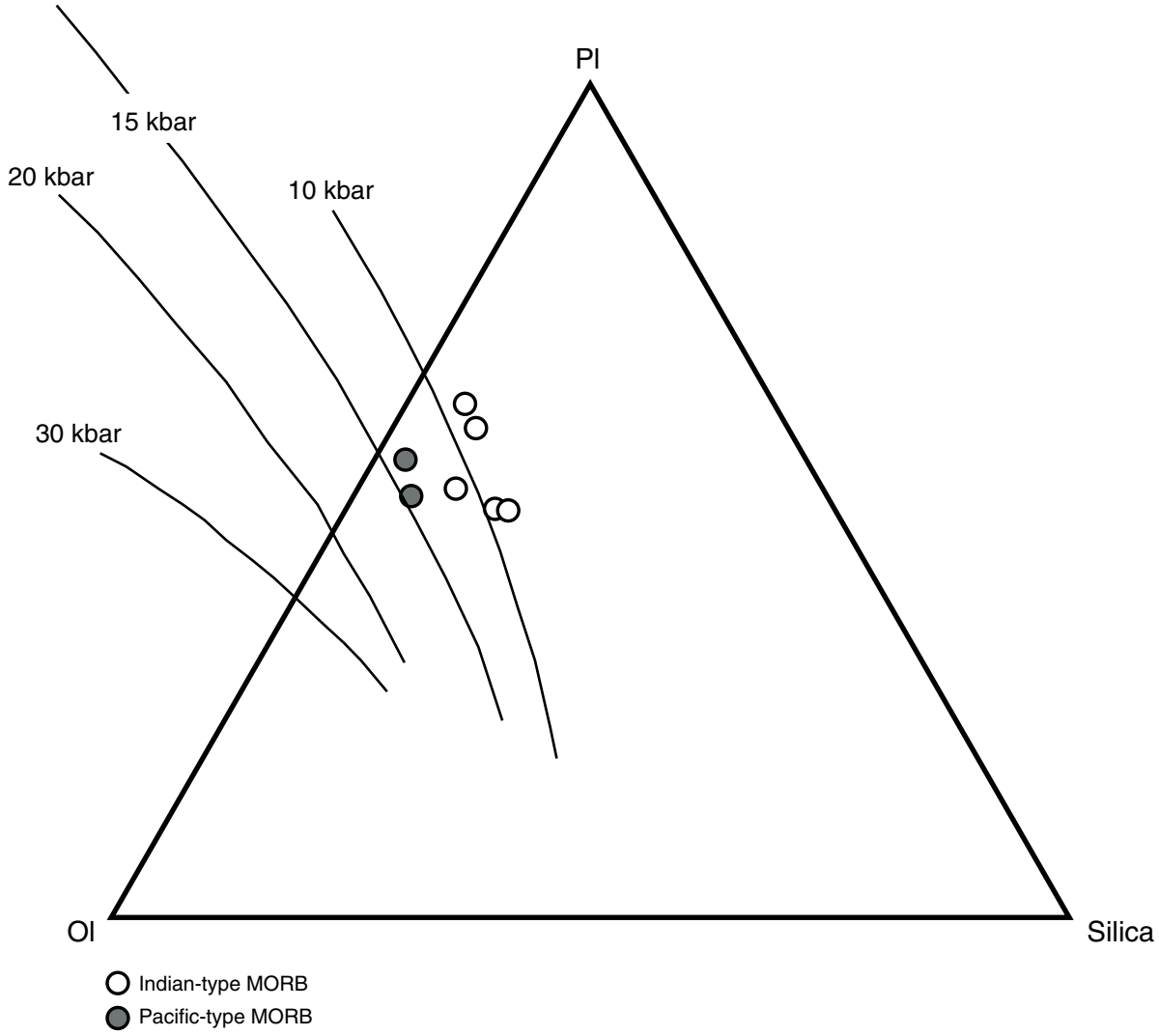

Figure F7. A schematic model for petrogenetic conditions at the AAD. Beneath Zone A, partial melting started and melts segregated deeper than was the case for the AAD. The length of the hypothetical melting column indicates the degree of partial melting.

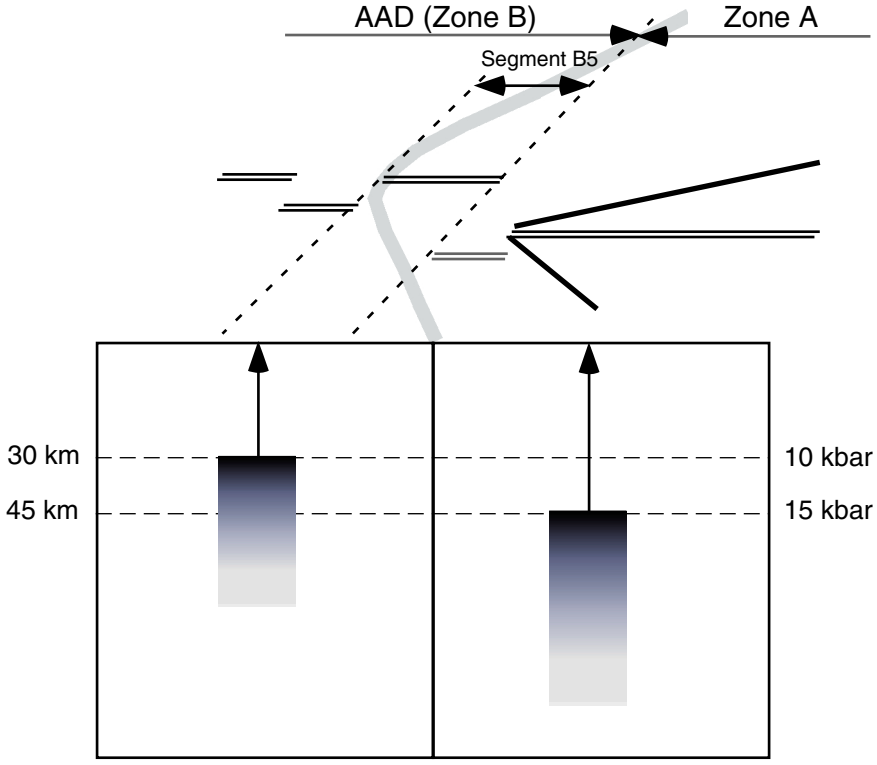

Table T1. Chemical compositions of olivine grains in lavas collected from ODP Leg 187. (This table is available in an **oversized format.**)

Table T2. Whole-rock and/or glass compositions for olivine maximum fractionation calculations.

MORB domain	Core, section, interval (cm)*	Core, section, interval (cm)†	Major element oxides (wt%)												Ni (ppm)	FeO‡/MgO	mg#	Method	Reference
			SiO_2	TiO_2	Al_2O_3	Fe_2O_3‡	FeO‡	MnO	MgO	CaO	Na_2O	K_2O	P_2O_5	Total					
Indian	187-1155A-5R-1, 13–17	187-1155A-5R-1, 20–23	51.96	1.69	14.88	11.05	9.94	0.18	8.01	10.81	3.15	0.25	0.22	102.20	99	1.24	0.59	Shipboard ICP-AES	Shipboard Scientific Party (2001)
Indian	187-1155B-4R-2, 65–67	187-1155B-4R-2, 22–26	50.18	1.06	17.40	8.71	7.84	0.15	8.18	11.91	2.68	0.25	0.11	100.62	156	0.96	0.65	Shipboard ICP-AES	Shipboard Scientific Party (2001)
Indian	187-1156A-2R-4, 14–16	187-1156A-2R-3, 133–136	51.66	1.41	15.63		8.71	0.16	8.29	11.63	2.69	0.12	0.14	100.45	111.7	1.05	0.63	EPMA/ICP-AES	Russo (this volume)
Indian	3R-2, 51–54	3R-2, 19–22	50.47	1.29	16.60	8.88	7.99	0.15	8.03	11.81	2.73	0.23	0.13	100.32	136	1.00	0.64	Shipboard ICP-AES	Shipboard Scientific Party (2001)
Indian	187-1161A-3R-1, 39–42	187-1161A-3R-1, 68–69	52.23	1.46	15.62	9.53	8.58	0.16	8.03	11.07	2.92	0.11	0.17	101.29	111	1.07	0.63	Shipboard ICP-AES	Shipboard Scientific Party (2001)
Pacific	187-1160B-4R-1, 48–52	187-1160B-4R-1, 59–62	49.20	1.19	15.34	9.83	8.85	0.15	8.86	11.93	2.67	0.07	0.09	99.99	129	1.00	0.64	Shipboard XRF	Shipboard Scientific Party (2001)
Pacific	9R-2, 11–14	9R-1, 125–129	49.45	1.04	15.77	9.48	8.53	0.13	8.90	12.25	2.50	0.04	0.07	100.34	104	0.96	0.65	Shipboard XRF	Shipboard Scientific Party (2001)

Notes: MORB = mid-ocean-ridge basalt. EPMA = electron probe microanalysis, XRF = X-ray fluorescence. * = olivine composition (this study). † = start compositions for calculation of melt compositions equilibrated with olivine composition. ‡ = total Fe as Fe_2O_3 for shipboard inductively coupled plasma–atomic emission spectroscopy (ICP-AES) analysis; for calculations, these values were recalculated to total Fe as FeO.

Table T3. Calculated compositions of primary melts and equilibrated olivine.

Hole:	187-1155A-	187-1155B-	187-1156A-		187-1161A-	187-1160B-	
Core, section:	5R-1	4R-2	2R-3	3R-2	3R-1	4R-1	9R-1
Interval (cm):	20–23	22–26	113–136	19–22	68–69	59–62	125–129
MORB province:	Indian	Indian	Indian	Indian	Indian	Pacific	Pacific
Step:	4	0	4	1	4	4	7
Equilibrated melt (wt%):							
SiO_2	50.97	50.30	51.01	50.66	51.60	49.66	49.49
TiO_2	1.61	1.06	1.35	1.28	1.40	1.16	0.98
Al_2O_3	14.14	17.44	14.95	16.53	14.96	14.99	14.90
FeO*	9.98	7.86	8.79	8.08	8.68	9.09	8.76
MnO	0.17	0.15	0.15	0.15	0.15	0.15	0.12
MgO	9.42	8.20	9.79	8.47	9.55	10.53	11.70
CaO	10.27	11.94	11.13	11.76	10.60	11.65	11.58
Na_2O	2.99	2.69	2.57	2.72	2.80	2.61	2.36
K_2O	0.24	0.25	0.11	0.23	0.11	0.07	0.04
P_2O_5	0.21	0.11	0.13	0.13	0.16	0.09	0.07
Ni (ppm)	168.0	156.0	188.6	156.9	190.0	209.7	234.9
Mg#	0.63	0.65	0.66	0.65	0.66	0.67	0.70
Equilibrated Ol composition:							
NiO (wt%)	0.296	0.321	0.328	0.313	0.339	0.342	0.351
Mg#	86.8	87.9	88.5	87.9	88.4	88.9	90.2
Norm ratio:							
Ol	51.3	50.8	46.9	48.1	46.5	55.5	56.5
Pl	34.9	39.4	32.4	39.1	30.4	40.2	35.4
Silica	13.9	9.8	20.7	12.8	23.1	4.3	8.1

Note: Ol = olivine, Pl = plagioclase.